Electronic Supplementary Material (ESI) for Lab on a Chip.

Supplementary Notes

Morphokinetics

Time-lapse data for full pre-implantation embryo development from fertilized oocytes denuded by manual pipetting (control), 80 MHz, or 200 MHz SAW. Exact post-insemination timing into 2nd polar body extrusion (tPB2), pronuclei appearance and fading (tPNa and tPNf), cleavage in to 2-cell to 8-cell (t2 to t8), morula compaction (tM), early blastulation (tSB), full blastocyst development (tB) and hatching (tHB) were recorded and compared.

Table 1. Comparison of timing of each embryo developmental stage

Timing (h)	**tPB2**	**tPNa**	**tPNf**	**t2**	**t3**	**t4**	**t5**	**t6**	**t7**	**t8**	**tM**	**tSB**	**tB**	**tHB**
Control	1.71 ± 0.59	5.04 ± 1.58	14.16 ± 0.99	16.19 ± 1.24	36.78 ± 2.72	38.18 ± 3.17	49.49 ± 3.88	51.49 ± 3.88	53.78 ± 6.75	58.82 ± 7.79	63.94 ± 6.13	75.26 ± 3.22	78.61 ± 2.66	88.13 ± 1.90
80 Mhz	1.97 ± 0.67	4.36 ± 0.74	14.47 ± 1.07	16.45 ± 1.10	35.93 ± 1.85	36.91 ± 1.98	47.11 ± 3.02	47.65 ± 3.11	48.53 ± 3.15	49.43 ± 3.24	57.45 ± 3.90	73.54 ± 1.46	77.35 ± 2.42	90.38 ± 3.85
200 Mhz	1.90 ± 0.65	4.35 ± 0.56	14.26 ± 1.09	16.17 ± 1.30	36.07 ± 2.50	37.30 ± 2.82	47.41 ± 3.71	47.98 ± 3.70	48.66 ± 3.62	50.27 ± 3.95	57.78 ± 4.98	77.03 ± 2.50	81.28 ± 4.25	88.91 ± 1.62

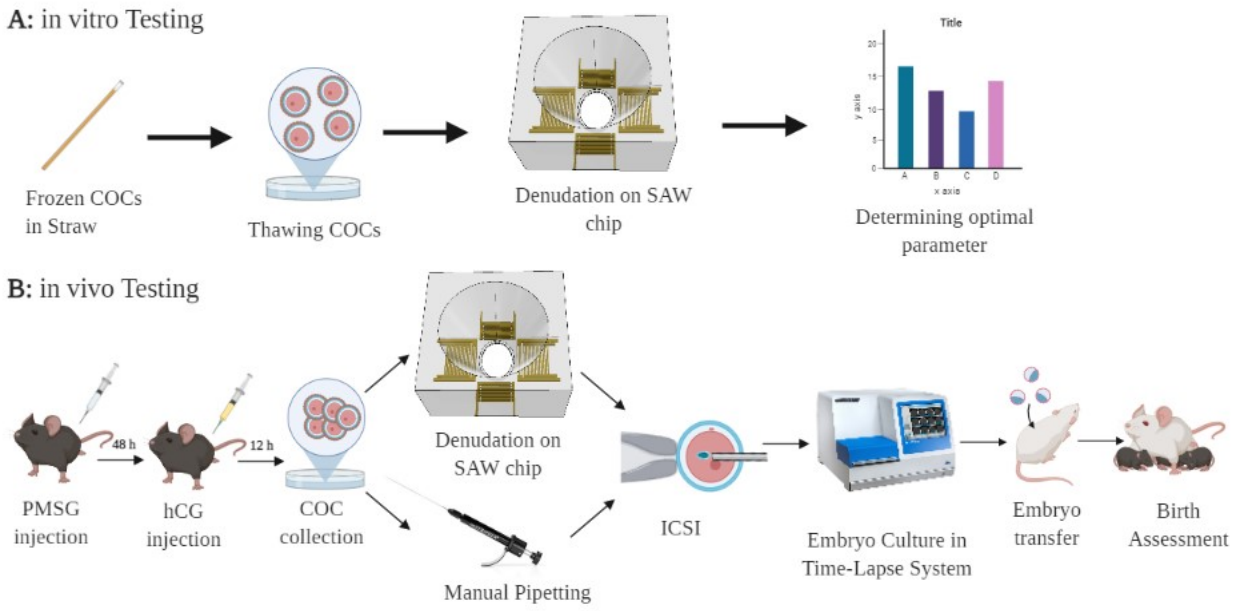

Figure 1. Schematics of experimental design. (A) in vitro testing protocol for device performance evaluation and parameter optimization (B) in vivo testing protocol for experimental evaluation of the safety of the devices on the development of embryos.

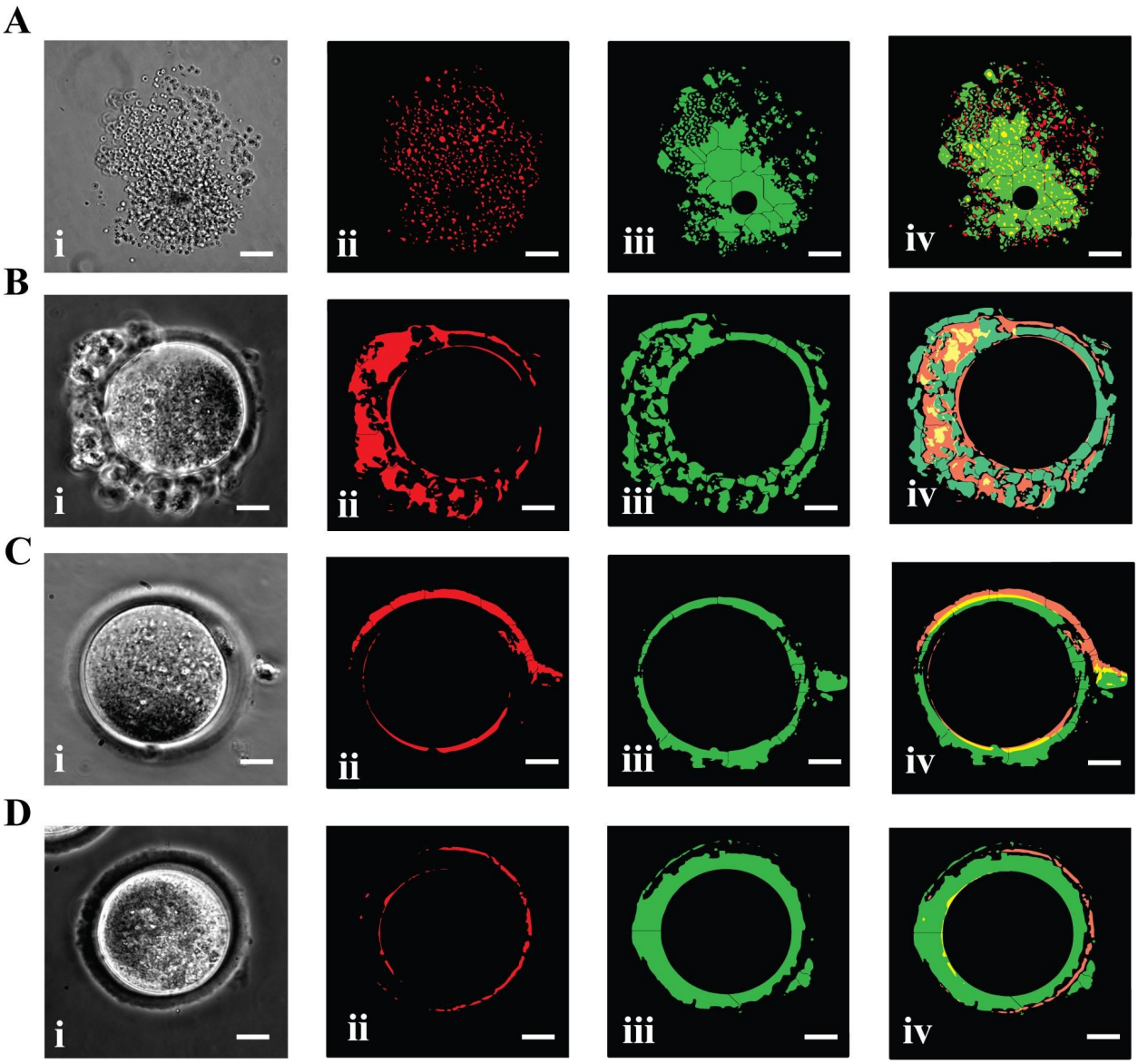

Figure 2. Image Segmentation results: A(i)-D(i) Original images taken with a phase-contrast microscope. A(ii)-D(ii) Segmented binary images capturing the darker ROI areas (than the background). A(iii)-D(iii) Segmented binary images capturing brighter ROI area. A(iv)-D(iv) final merged masks indicating the total cumulus area surrounding the oocyte. The yellow color shows the overlap between the dark and bright masks. Scale bar in A is 150 microns and Scale bars in B-D are 25 microns.

Calculation of body force on the liquid

According to the theory of acoustic streaming a sound wave damps upon entering a liquid through relaxational dissipation.[1] Consequently, a volumetric force, as a function of frequency-dependent absorption coefficients, acts on the body of the liquid in the direction of wave propagation. For example, a plane wave propagating in the x-direction with an amplitude of A

and damping length of l_a can be described as $U = Ae^{\frac{x}{l_a}}cos(\omega t - kx)$. The force is then given by $F_x = \rho_0 A^2 e^{\frac{2x}{l_a}}/l_a$ in which amplitude can be calculated from power and surface area from $P = \frac{1}{2}c\rho_0 A^2 n \cdot s$. By substitution, the force in the x-direction simplifies to $F_x = \frac{2P}{cSl_a cos(\theta)}e^{\frac{2x}{l_a}}$ which reveals a linear relationship between force and acoustic power.[2] Due to the linear relationship of electric power and acoustic power, with Stokes equations governing the fluid flow, a linear relationship between the fluid flow and applied power is expected. Assuming the primary mechanism of denudation is from the shear of the drag forces, such linearity is observed between the denudation efficiency as a function of applied power. (Fig.6A)

SAW denudation Module fabrication

SAW chip fabrication

We chose 128° Y-cut lithium Niobate $(K^2 = 5.3\%)$ with a reduced pyroelectric coefficient as substrate material because of its higher electromechanical coefficient. We used a lift-off process for transferring patterns on top of the substrate. A thin film of Ti/Au (200 nm/10 nm) was deposited using the E-beam evaporation process on a substrate patterned with a negative tone photoresist (nLoF-2020). After lift-off cleaning, the substrate was diced and glued to the printed circuit board (PCB) using a very thin epoxy layer. After securing the SAW substrate on the PCB, electrical connections were made using a wire bonding technique. In order to prevent unwanted wire detachments during the denudation procedure and minimize spurious electrical fields, we covered the wire bonds with potting epoxy. The potting epoxy was intentionally applied very close to the end of its working time window (at high viscosity) to minimize its spread on the substrate. The SAW chip fabrication steps are illustrated in Fig. S3B.

Micro-well fabrication steps

The micro-milling technique is used for the fabrication of the layers necessary for microwell production. Due to the wide angle of the microwell attached to the substrate, it is not possible to remove the PDMS layer from the substrate. As such, the microwell master is fabricated in two pieces that could be assembled like Lego pieces as illustrated in Fig. S3A. After assembly, the PDMS is poured on the master substrate until it is slightly lower than the microwell height such that the microwell top surface remains exposed to the air. This technique allows for the removal of the microwell piece without puncturing the PDMS layer and allows the pieces to be reusable. It is worth mentioning that theoretically, the height of the fringe that defines the bottom geometry of the microwell should be the same height as the sections covering the IDTs to assure complete sealing. However, even when the height of the fringe is slightly smaller than the gap covering the IDT sections, preventing it from touching the substrate, the resulting structure

automatically prevents the medium leakage by creating an expansion zone that acts like microfluidic stop valves.[3] This works to our advantage, making the microfabrication process less sensitive to slight height variations. However, applying higher actuation power >30 dBm can overcome the Laplace pressure and draw the liquid over the IDTs, leading to actuation attenuation.[4]

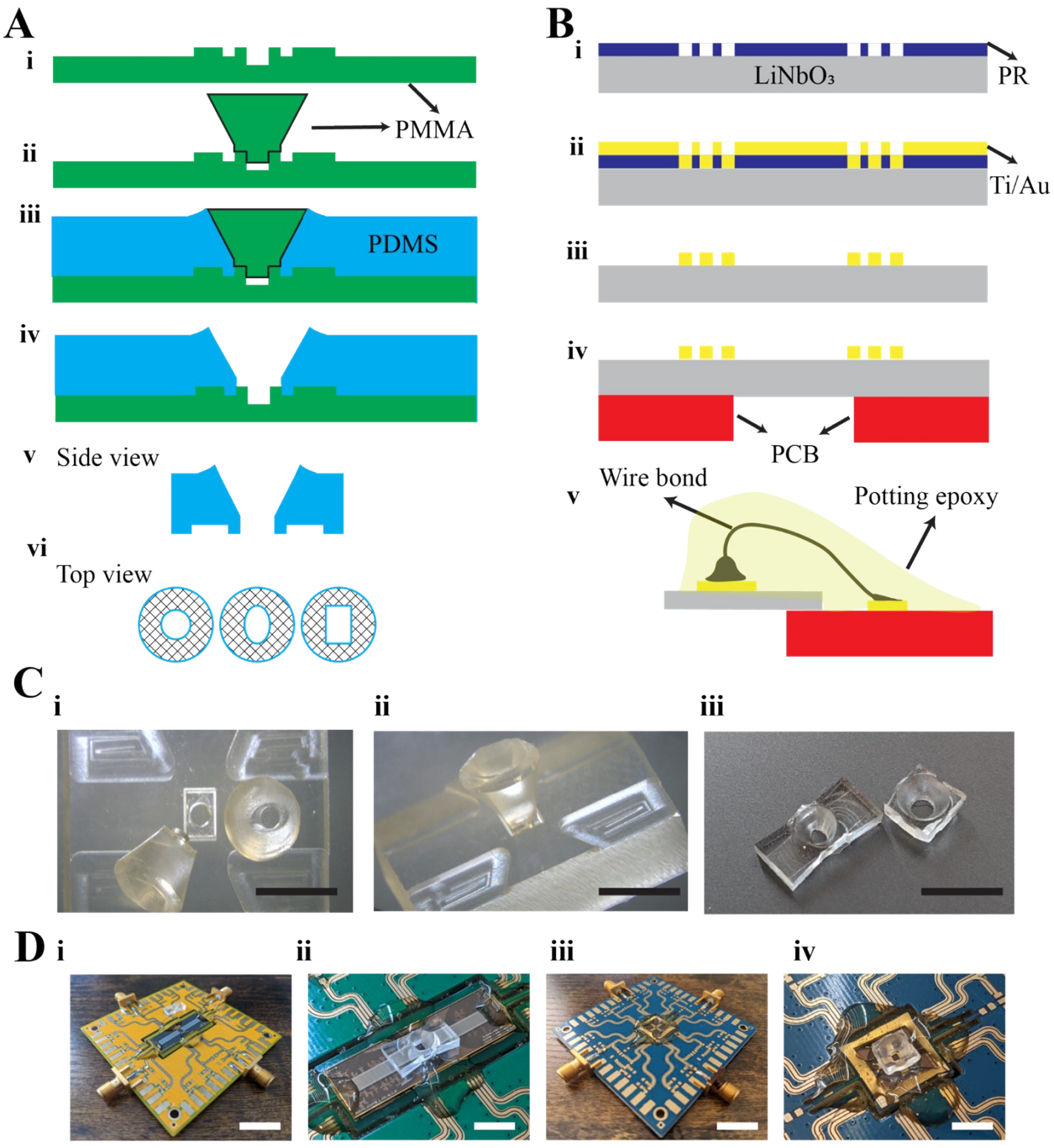

Figure 3. A Fabrication process of the microwell parts. (i-ii) shows the PMMA parts and their assembly like Legos (iii-v) shows the soft lithography process. (vi) Microwells with different

contact area geometry have a hydraulic diameter of 2-2.5 mm and a height of 3 mm B fabrication process of SAW devices. (i-iii) shows IDT and electrode patterning on a lithium niobate substrate. (iv-v) shows mounting of the dies on PCB and wire bond securing using epoxy. C (i) top view image of microwell parts (ii) perspective view of the assembled microwell parts. (iii) The final PDMS microwells for the “dry” and “wet” configurations. D The perspective and close up images of assembled (i-ii) “dry” and (iii-iv) “ wet” state devices.

Electrical characterization of SAW

We chose an ultrasound resonant design for x and y directions to also benefit from the Q factor to increase the efficiency (scale factor) of the device. In addition, we also added the thin-film metallic short reflector gratings in the x-direction to confine the main ultrasound beam to the acoustic cavity and reduce leakage losses. This easy to fabricate method introduces small acoustic impedances at the metal deposited locations and if their number reaches the critical reflecting element number (N_R), they can reflect most of the incident waves back to the acoustic cavity. As such >300 reflecting elements calculated based on the Sitting method [5] were added to reflect most of the incident wave back. We measured the resonant frequency of the devices by measuring the SAW scattering parameters using a Keysight E5061B analyzer. The S_{21} parameter, comparing the transmission from input to output for each direction, is shown in Fig. S4B. Resonant frequency shift measured for x directions due to temperature variation either do to fluctuation induced by the attached heater or due to the thermal effects induced by the SAW itself is shown in Fig. S4A. The corresponding resonant frequencies, wavelengths, and damping lengths are listed in Table S2.

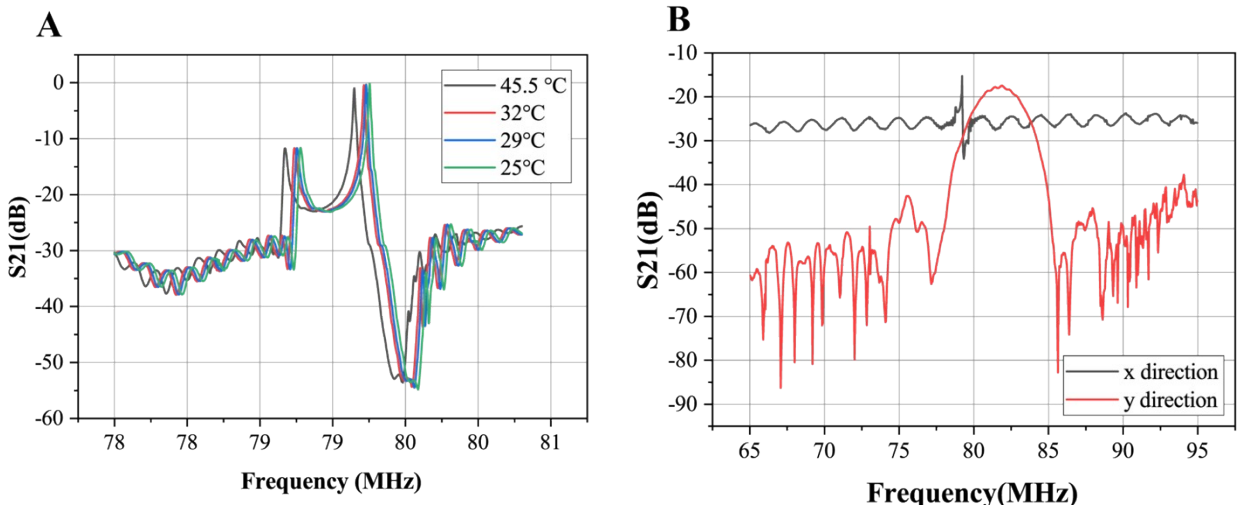

Figure 4. (A) S21 parameter shifts due to temperature increase by the attached heater below the substrate. (B) S21 parameters for x-direction with reflector gratings and y-direction without reflectors. The reflectors in the x-direction result in a narrower bandwidth compared to the y-direction allowing switching of the wave propagation with slight frequency change without using RF switches.

Table 2. Corresponding resonant frequencies, actual wavelengths, and damping (attenuation) lengths (xs,xf) listed for each propagation direction.

	Frequency, actual *f,* **MHz**	Wavelength on SAW [*μm*]	Wavelength in water [*μm*]	Damping length on SAW, x_s [*μm*]	Damping length in water x_f [*mm*]
x direction	79.29	50.3090	18.8927	279.6796	10.1375
y direction	81.19	49.1317	18.4505	273.1346	9.6686
x direction	199.14	20.0311	7.5223	111.3578	1.6071
y direction	202. 21	19.7270	7.4081	109.6672	1.5587
$\square_{saw}$ = 3989 m/s and $\square_F$ = 1498 m/s [2]					

Electrical Effects

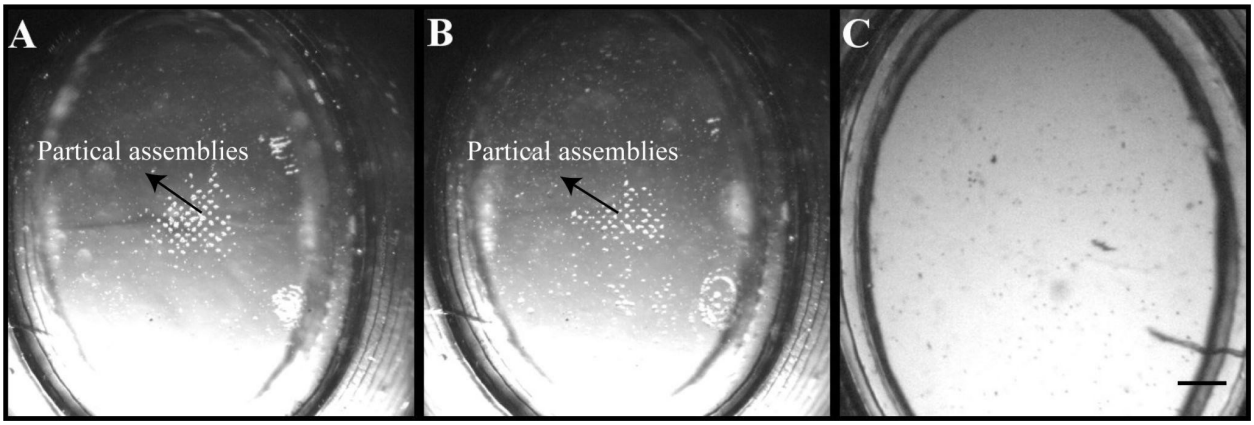

Figure 5. (A) One-micron particle assembly at the bottom of the microwell in a “dry” state device when driven with a CW signal at 23 dBm using deionized water. (B) One-micron particle assembly at the bottom of the microwell in a “dry” state device when driven with a CW signal at 23 dBm using an M2 culture medium. (C) Driving “wet” state device at off-resonant frequencies at a higher power of 30 dBm using either of the deionized water of medium without a one-micron particle assembly.

Lithium niobate birefringence and Image quality

The lithium niobate used as the piezo substrate of the acoustic denudation module is a negative uniaxial crystal (double refracting crystal). The axial birefringence in lithium niobate crystals

induces splitting in transmission optical images in an inverted microscope setup, resulting in the creation of twin images.[6,7] Using a polarizer to eliminate one of the twin images results in light scarceness, decreasing the light intensity by half and lowering the image quality as can be seen in Fig. S6. Surprisingly, although the amount of decreased light can be compensated for by increasing the amount of the incoming light, the image quality remains lower compared to the glass substrate, eventually compromising the image processing steps. As such, the same denudation mechanism can be applied using other actuation mechanisms. For example, using BAW mode ultrasonics with piezoelectric ceramics or electromagnetic actuation of a transparent membrane with embedded micromagnets, which eliminates the need for special substrates resulting in even lower fabrication costs.

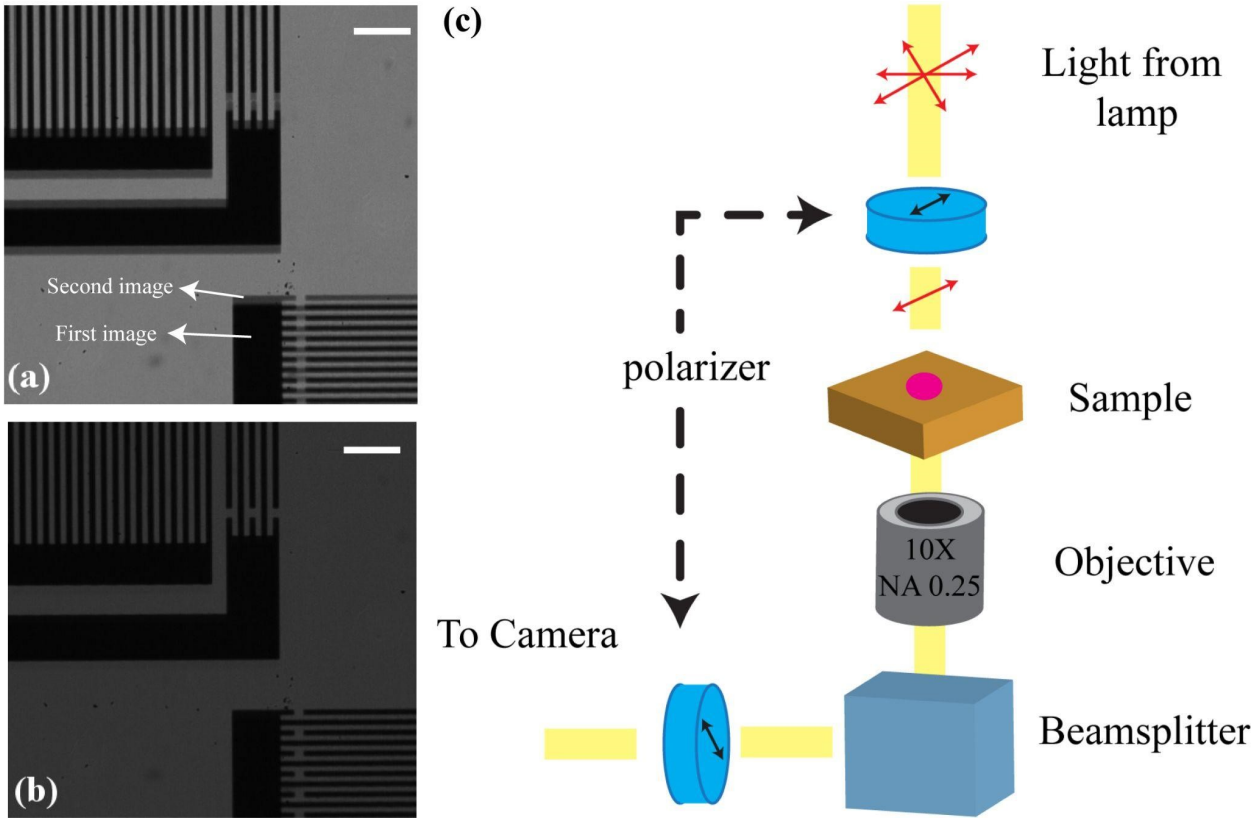

Figure 6. (a) Twin images as a result of lithium niobate crystal birefringence. (b) Light intensity decrease and twin image elimination by using a polarizer. (c) Polarizer placement on either top of the sample or before the camera in imaging setup eliminates the twin image. The amount of reduced light intensity can be compensated by increasing the illumination.

Movie captions

Movie S1. Flow patterns in “dry” state devices with circular and elliptical microwells. Fluidic patterns revealed by mixing a high density fluidic (OptoPrep media) with deionized water. The

scale bar is 800 microns. Foldings are clearly seen upon shifting the resonant frequency from x to y-direction.

Movie S2. CW vs SFM mode signal actuation of a “dry” state device with an elliptical base microwell. In CW mode, 15-micron particles assemble in specific patterns while applying an SFM mode signal to achieve complete mixing inside the microwell without creating any specific patterns.

Movie S3. 100-microns particles’ trajectories in a “dry” state device actuated with (A) a CW signal in the x-direction. (B) an SFM signal. 100-microns particles’ trajectories in a “wet” state device actuated with (A) a CW signal in the x-direction. (B) cell trajectories in a “wet” state device derived with an SFM signal.

Movie S4. Representative demonstration of *in vitro* testing protocol. A-D shows 10 seconds of the operation from loading to complete denudation consecutively.

Movie S5. Representative demonstration of *in vivo* testing protocol for both “dry” and “wet” state devices showing complete denudation of multiple oocytes.

Movie S6. Representative demonstration of a big cluster of fresh COC denudation on a “wet” state device and gradual detachment of single COCs from the cluster.

Movie S7. Representative time-lapse imaging videos of oocytes denuded with both “dry” and “wet” state devices for morphokinetics embryo development evaluation.

Movie S8. Representative Piezo-ICSI performance on denuded oocytes.

References

1 S. J. Lighthill, *J. Sound Vib.*, 1978, **61**, 391–418.

2 L. Schmid, A. Wixforth, D. A. Weitz and T. Franke, *Microfluid. Nanofluidics*, 2012, **12**, 229–235.

3 A. Olanrewaju, M. Beaugrand, M. Yafia and D. %J L. on a. C. Juncker, 2018, **18**, 2323–2347.

4 A. R. Rezk, O. Manor, J. R. Friend and L. Y. Yeo, *Nat. Commun.*, 2012, **3**, 1167.

5 E. K. Sittig and G. A. Coquin, *IEEE Transactions on Sonics and Ultrasonics*, 1968, **15**, 111–118.

6 L. Arizmendi, *Physica Status Solidi A Appl. Res.*, 2004, **201**, 253–283.

7 A. A. Nawaz, M. Urbanska, M. Herbig, M. Nötzel, M. Kräter, P. Rosendahl, C. Herold, N. Toepfner, M. Kubánková, R. Goswami, S. Abuhattum, F. Reichel, P. Müller, A. Taubenberger, S. Girardo, A. Jacobi and J. Guck, *Nat. Methods*, 2020, **17**, 595–599.